Dual Energy CT of the Chest

How About the Dose?

Jan C. Schenzle, Wieland H. Sommer, MD,* Klement Neumaier,† Gisela Michalski,† Ursula Lechel, MS,‡ Konstantin Nikolaou, MD,* Christoph R. Becker, MD,* Maximilian F. Reiser, MD,* and Thorsten R. C. Johnson, MD**

Objective: New generation Dual Source computed tomography (CT) scanners offer different x-ray spectra for Dual Energy imaging. Yet, an objective, manufacturer independent verification of the dose required for the different spectral combinations is lacking. The aim of this study was to assess dose and image noise of 2 different Dual Energy CT settings with reference to a standard chest scan and to compare image noise and contrast to noise ratios (CNR). Also, exact effective dose length products (E/DLP) conversion factors were to be established based on the objectively measured dose.

Materials and Methods: An anthropomorphic Alderson phantom was assembled with thermoluminescent detectors (TLD) and its chest was scanned on a Dual Source CT (Siemens Somatom Definition) in dual energy mode at 140 and 80 kVp with 14 × 1.2 mm collimation. The same was performed on another Dual Source CT (Siemens Somatom Definition Flash) at 140 kVp with 0.8 mm tin filter (Sn) and 100 kVp at 128 × 0.6 mm collimation. Reference scans were obtained at 120 kVp with 64 × 0.6 mm collimation at equivalent CT dose index of 5.4 mGy*cm. Syringes filled with water and 17.5 mg iodine/mL were scanned with the same settings. Dose was calculated from the TLD measurements and the dose length products of the scanner. Image noise was measured in the phantom scans and CNR and spectral contrast were determined in the iodine and water samples. E/DLP conversion factors were calculated as ratio between the measured dose form the TLDs and the dose length product given in the patient protocol.

Results: The effective dose measured with TLDs was 2.61, 2.69, and 2.70 mSv, respectively, for the 140/80 kVp, the 140 Sn/100 kVp, and the standard 120 kVp scans. Image noise measured in the average images of the phantom scans was 11.0, 10.7, and 9.9 HU ($P > 0.05$). The CNR of iodine with optimized image blending was 33.4 at 140/80 kVp, 30.7 at 140Sn/100 kVp and 14.6 at 120 kVp. E/DLP conversion factors were 0.0161 mSv/mGy*cm for the 140/80 kVp protocol, 0.0181 mSv/mGy*cm for the Sn140/100 kVp mode and 0.0180 mSv/mGy*cm for the 120 kVp examination.

Conclusion: Dual Energy CT is feasible without additional dose. There is no significant difference in image noise, while CNR can be doubled with optimized dual energy CT reconstructions. A restriction in collimation is required for dose-neutrality at 140/80 kVp, whereas this is not necessary at 140 Sn/100 kVp. Thus, CT can be performed routinely in Dual Energy mode without additional dose or compromises in image quality.

Key Words: dual energy CT, radiation exposure, image noise, contrast to noise ratio, lung perfusion

(*Invest Radiol* 2010;45: 347–353)

Received September 20, 2009; accepted for publication (after revision) January 19, 2010.

From the *Departments of Clinical Radiology, and †Radiotherapy and Radiooncology, University Hospitals-Grosshadern, Ludwig-Maximilians University, Munich, Germany; and ‡Federal Office for Radiation Protection, Department of Medical Radiation Hygiene and Dosimetry Helmholtz-Zentrum, Neuherberg, Germany.

The authors J. C. S. and W. H. S. contributed equally to the study.

Reprints: Thorsten R. C. Johnson, MD, Department of Clinical Radiology, University of Munich, Grosshadern Campus, Marchioninistr 15, 81377 Munich, Germany. E-mail: thorsten.johnson@med.uni-muenchen.de.

ISSN: 0020-9996/10/4506-0347

The rapid advances in computed tomography (CT) continuously improve image quality and diagnostic accuracy. The robustness and speed of the modality entails a wide and growing spectrum of clinical indications. However, the consistently increasing use of ionizing radiation and the growing total dose to the population have triggered concerns about cancer risk and sparked off a trend to new dose-saving techniques.[1] In Germany, CT examinations represent about 7% of all x-ray examinations (2004) but account for more than 54% of the resultant total effective dose.[2] Therefore, any new CT technology that may require an additional radiation exposure has to be regarded with caution.

A new generation of CT scanners integrating 2 x-ray sources and detectors in one gantry with an angular offset of about 90° has increased the temporal resolution by a factor of 2[3,4] and thus brought about a new reliability of cardiac imaging.[5,6] Also, this system design makes spectral imaging, ie, Dual Energy CT (DECT), feasible in clinical routine.[7] This technique is based on the acquisition of 2 CT datasets with 2 different x-ray spectra which are generated with different tube voltages and filters. The images are reconstructed separately from the projection data of both detectors and can be used to identify certain substances with spectral properties, eg, iodine or xenon gas. The imaging data from both detectors can also be averaged into one image, generating a dataset similar to a standard 120 kV acquisition, but this is only possible for the field of view (FOV) covered by both detectors with a maximum coverage of 33 cm diameter. There are multiple applications for DECT, and several studies have shown clinical benefits as the exact identification of renal stones,[8–10] detection and characterization of liver or kidney neoplasm,[11–13] assessment of myocardial perfusion,[14] visualization of lung perfusion or ventilation,[15–18] or bone removal from angiographic datasets.[19–21] Several other fields of application are still being developed and evaluated.

In the early development of DECT, its clinical value was still unclear and an additional radiation exposure not justified. Therefore, DECT protocols were set such that the CT dose index, ie, the dose applied to a certain range, approximately equals that of a normal CT scan of the individual area of the body. To achieve comparable noise levels, the tube currents of both tubes were adapted with a certain relation, because the efficiency in output of x-ray quanta is highly energy dependent.[7] The 80 and 140 kVp are routinely used because these voltages are achievable with the x-ray tubes and generate an adequate difference in attenuation. Still, the spectral difference is limited by the broad overlap of the 2 x-ray spectra (Fig. 1). Moreover, the limited transmission of 80 kVp quanta in dense areas of the body such as the shoulders, the pelvis, or the abdomen requires a thicker collimation if no additional dose is to be administered.[11,22]

A new 0.4 mm thick tin (Sn) filter was implemented in the new version of the Siemens DSCT scanner (Siemens Definition Flash) to rid the 140 kVp spectrum of low-energy quanta and to further separate the spectra so that a similar spectral contrast can be

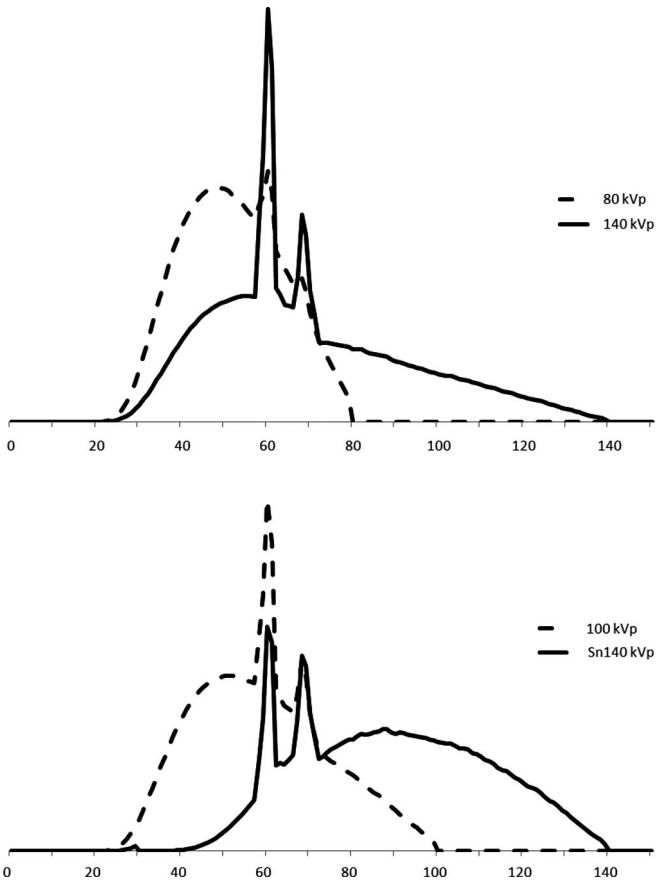

FIGURE 1. Photon energy spectra of the x-ray tubes operating at 80 and 140 kV potential are shown in red and blue, and the spectrum of a tube running at 140 kVp with additional 0.4 mm tin filter (SPS, selective photon shield) shown in green. Note the significantly smaller overlap between the 80 and Sn140 kVp spectra (Source of Monte Carlo simulation data: Siemens Healthcare, Forchheim, Germany).

obtained with a combination of the filtered Sn-140 kVp and a 100 kVp spectrum.[23] Thus, insufficient transmission of thin 80 kVp projections in large or dense objects such as the abdomen is avoided, and a thin 0.6 mm collimation can be used.

The purpose of this study was to assess dose and image noise of different DECT protocols in manufacturer independent, objective measurements with thermoluminescent dosimeters, compared with a standard pulmonary CT angiography scan for reference. Additionally, the contrast to noise ratio (CNR) of spectral information was to be determined with different combinations of x-ray spectra using iodine and water samples. A further purpose was to assess the performance of nonlinear blending algorithms, which are useful to optimize contrast information in CT images derived from DECT. Furthermore, exact effective dose length products (E/DLP) conversion factors were to be established based on the objective dose information from the thermoluminescent detectors (TLD).

Overall, the question to be answered was, whether DECT requires additional dose compared with conventional CT or not, also taking compromises in collimation or image noise into account.

FIGURE 2. Scan range for the chest, covering the entire lungs and mediastinum, the lower neck, the domes of the diaphragms, and a part of the upper abdomen. The scan length in all protocols was kept equal with 276 mm.

MATERIALS AND METHODS

TLD Preparation

For objective dose measurements independent from manufacturer calibration, thermoluminiscent detectors (TLD) were used. The main component of a TLD is a combination of lithium and fluorine doped with magnesium and titanium. When a crystal lattice like lithium and fluorine is irradiated, electrons are emitted and trapped by the impurity of magnesium and titanium. These trapped electrons represent the amount of measured radiation and can be read-out up to 24 hours after exposure without loss of information. TLDs were primarily developed for radiotherapy and are designed to measure radiation in the range of one or several Grays (Gy). To measure dose in TLDs, a complex prearrangement is necessary, including cumulating calibration factors. To generate these factors, each TLD was exposed to exactly 1 Gy using a ^{137}CS source and subsequently read out to obtain the measured TLD dose, standard deviations and its sensitivity.

Alderson Rando Phantom Assembly

The TLDs were placed in an anthropomorphic Alderson-Rando phantom representing a 175 cm tall, 73.5 kg male patient with a thoracic diameter of 32 cm (Alderson Research Laboratories Inc., Stanford, CT). The phantom was equipped with 58 thermoluminescent dosimeters with dimensions of 1 × 1 × 6 mm (TLD-100H, Bicron Harshaw, Radiation Measurement Products, Cleveland, OH). Each TLD position was carefully selected in the region of interest for a thoracic scan, considering the scan range and the additional range potentially affected by scatter radiation (Fig. 2). To evaluate specific organ doses and account for z-axis variability for each scan protocol, the TLDs were allocated to every organ in several slices in the scan range:

Lung (n = 14), thyroid gland (n = 1), esophagus (n = 4), vertebral spine (n = 5), mediastinum (n = 4), liver (n = 6), stomach (n = 1) colon (n = 1), and skin (n = 22).

TLD Exposure

To assess effective radiation dose, E/DLP conversion factors, noise and CNR, the Alderson phantom was scanned on Dual Source CT scanners using 3 different scan protocols:

TABLE 1. CT—Parameter Settings of the Dual Energy and Conventional 120 kVp Chest Protocols

Protocol	Dual Energy Scan Definition	Dual Energy Scan Definition Flash	Standard Chest Scan Definition Flash
Voltage tube A (kVp)	140	100	120
Voltage tube B (kVp)	80	Sn140	
Reference current-time product tube A (mAs)	80	165	160
Reference current-time product tube B (mAs)	340	140	
Effective current-time product tube A (mAs)	30	73	90
Effective current-time product tube B (mAs)	117	68	
CT dose index with CareDose4D (mGy)	5.37	5.37	5.89
Scan length (mm)	276	276	276
Pitch	0.7	0.55	1.2
Gantry rotation time (sec)	0.5	0.28	0.5
Collimation (mm)	14 × 1.2	128 × 0.6	128 × 0.6
Reconstructed slice thickness/position increment (mm)	2	2	2
Kernel	D30f	D30f	D30f

1. Dual Energy pulmonary CT angiography protocol at 140/80 kVp.
2. Dual Energy pulmonary CT angiography protocol at Sn140/100 kVp.
3. Single Energy pulmonary CT angiography protocol at 120 kVp.

Detailed scan parameters are listed in Table 1. The first protocol was performed on a Dual Source CT (Siemens Somatom Definition, Forchheim, Germany) in dual energy mode at 140 and 80 kVp with 14 × 1.2 mm collimation. The same was applied on a second generation Dual Source CT scanner (Siemens Somatom Definition Flash, Forchheim, Germany) at 140 kVp with 0.4 mm tin filter (Sn) and 100 kVp at 128 × 0.6 mm collimation. Reference scans were obtained at 120 kVp with 128 × 0.6 mm collimation at equivalent volume CT dose index (pitch corrected CTDIvol) of 5.4 mGy*cm, also on the Definition Flash scanner. To compare dose efficiency, the same dose was to be applied with all 3 protocols. To achieve a higher total radiation exposure and to minimize statistical variations, all scan protocols were repeated 10 times with constant parameter settings. Therefore, the tube current was adjusted such that the user interface showed a CTDIvol of 5.4 mGy*cm.

TLD Read-Out

To read out the TLD after exposure, each Rod was heated to 350 centigrade using a nitrogen flow. With heating, the trapped electrons in the TLD emit a characteristic glow curve when switching their atomic energy level. This is detected by a photomultiplier and converted to the specific amount of absorbed radiation. The read out procedure consisted of the following steps:

1. Sorting TLD to a carrier plate.
2. Read-Out process using a TL-Detector 2000D (Harshaw Radiation Measurement Products, Cleveland, OH) to generate specific glow curves and a TL Picoprocessor 2080 (Harshaw) to convert to dose.
3. TLD Storage deletion using a TLDO Annealing Oven (PTW, Freiburg, Germany).

Dose Calculation

Dose was calculated from the TLD measurements and the appropriate organ weighting factors,[24] and specific conversion coefficients were calculated from the dose length products of the scanner.

The overall dose was calculated from the individual doses of the TLDs in one organ. The effective dose of the chest was calculated by multiplying the sum of the absorbed organ dose with its appropriate tissue weighting factor according to ICRP-103.[24] Lung, esophagus, and mediastinum are fully covered in the scan range and their dose was entirely taken into account. At the ends of the scan range, the partial coverage of the individual organ in the scan range was taken into account by estimating the exposed share of the organ in relation to its total size. Several organs in the scan area including the heart, the mediastinal lymph nodes, the pararenal glands, and the pancreas, are not assigned to a specific conversion factor in ICRP-103[24] but are summed in the "remainder tissues" parameter which also contains several other organs. We estimated a share of 40% of these organs to be exposed. The percentages used for the other organs are listed in Table 2.

E/DLP Conversion Factors

To determinate E/DLP conversion factors X, the measured effective doses (D_E) from the TLDs and the dose length product (DLP) from the patient protocol were divided:

$$X = \frac{D_E(\text{mSv})}{\text{DLP}(\text{mGy} \times \text{cm})}$$

Noise Measurements

Images were reconstructed from every acquisition using a D30f convolution kernel and a slice thickness and increment of 2 mm (Fig. 3). To achieve similar spectral properties, average images were reconstructed from the dual energy CT acquisitions with weighted contributions from both detectors, ie, applying the standard weighting factor of 0.3 to include 70% of density information from the 140 kVp dataset and 30% from the 80 kVp acquisition. With the combination of the filtered 140 kVp and the 100 kVp spectra, average images were reconstructed with equivalent contributions from both detectors, ie, with the standard weighting factor of 0.5. These weighting factors imply a linear blending, ie, every image voxel contains density information from both datasets with a fixed linear relation.

For noise measurements, 14 regions of interest (ROI) at 7 different z-axis positions were chosen inside the phantom in a homogeneous area of the mediastinum. A standardized ROI size of 4.20 cm^2 and equivalent positions were used for all acquired protocols. Noise was calculated for each acquisition protocol as the average standard deviation of CT numbers in all regions of interest.

TABLE 2. TLD Measurement Results With the Corresponding Partial Doses at Current Organs Including the Organ Specific Weighting Factors for All Three Protocols

Measured Dose (mSv)					
Organ	**Definition (140/80 kVp)**	**Definition Flash (Sn140/100 kVp)**	**Standard Chest (120 kVp)**	**Weighting Factor (ICRP103)**	**Share Exposed**
Thyroid gland	0.21	0.27	0.18	0.04	50%
Lung	0.99	0.99	1.06	0.12	100%
Esophagus	0.34	0.33	0.37	0.04	100%
Bone marrow	0.28	0.28	0.30	0.12	33%
Bone surface	0.02	0.02	0.02	0.01	33%
Remainder tissues*	0.41	0.39	0.46	0.12	40%
Liver	0.10	0.10	0.06	0.04	50%
Stomach	0.19	0.23	0.19	0.12	50%
Colon	0.052	0.064	0.045	0.12	20%
Skin	0.014	0.014	0.015	0.01	18%
Total	2.606	2.688	2.700		

*Remainder tissues contain adrenals, extrathoracic (ET) region, gall bladder, heart, kidneys lymphatic nodes, muscle, oral mucosa, pancreas, prostate, small intestine, spleen, thymus, uterus/cervix.

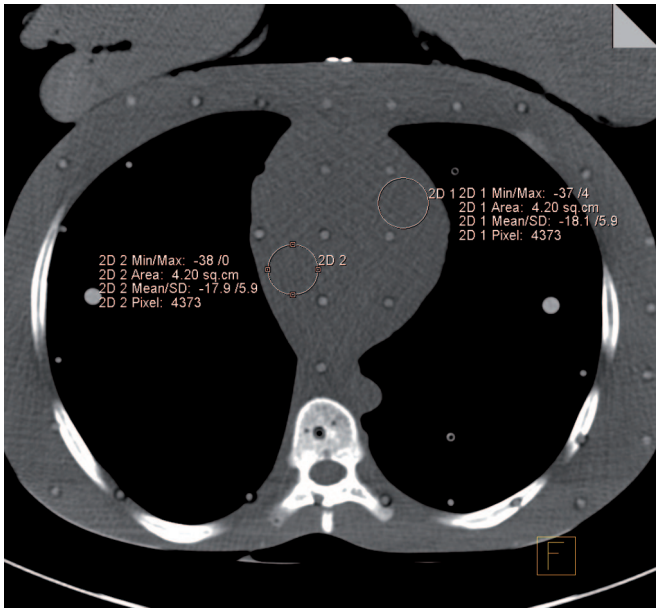

FIGURE 3. Example for density measurements. Two ROIs are placed in a homogeneous area of the phantom's mediastinum.

Contrast to Noise Ratio Measurements

To quantify the CNR, which is more relevant for the diagnostic evaluation than image noise, phantom measurements with iodine and water were performed. Two syringes were filled, one with a mixture of contrast material and saline (concentration 17.5 mg iodine/mL comparable to the concentration in blood in an angiographic examination) and one with saline solution (NaCl 0.9%). The syringes were placed on the chest of the Alderson phantom, surrounded by a water bag with a layer of about 2 cm of water on top of the syringes to limit beam hardening. The different protocols mentioned above were performed with equal settings, and images were reconstructed using the same kernel and slice thickness. Two ROI were measured in the lumen of both syringes at 4 different z-axis positions.

To quantify the CNR, 3 different calculation approaches were used. First, to evaluate general image quality, a general CNR was determined in average images of the dual energy acquisitions and in the standard 120 kVp images. These CNR values were calculated as quotient of the mean value of CT numbers of the contrast material in the syringe and the image noise, ie, its standard deviations.

To evaluate the performance of nonlinear blending algorithms, optimized images were additionally reconstructed using an US Food and Drug Administration approved software (Syngo Dual Energy optimum contrast, Siemens).[25] This software loads both the high and low energy dataset and optimizes contrast and noise in the image. This is achieved by variably adding different relations of density information from both datasets, limiting noise in homogeneous areas with data from the high energy image and improving contrast in areas containing iodine by adding more information from the low energy image. In the resulting images, CNR was determined in the same manner.

Additionally, the spectral contrast in Dual Energy images was determined to quantify the spectral separation. The CNR value was calculated as the difference between the CT numbers in the center of the iodine syringe at Sn140 kVp and 100 kVp, divided by the background noise. The CNR was also calculated for images at 140 kVp and 80 kVp.

Statistics

The significance of differences between noise values or CNR was tested using an analysis of variance (ANOVA). In case of significant results of the ANOVA, posthoc t-tests for unpaired samples were used. In case of multiple comparisons, the *P* value was corrected according to Bonferroni.

RESULTS

Dose Length Products

The dose length products in the patient protocols were 143 mGy*cm for the 140/80 kVp examination on the Somatom Definition, 165 mGy*cm for the Sn140/100 kVp protocol and 146 mGy*cm for the 120 kVp single-source scan on the Somatom Definition Flash. Using a standard conversion factor of 0.017 mSv/mGy*cm[26] for the chest in literature to estimate effective Dose, these values would correspond to 2.43, 2.80, and 2.48 mSv, respectively (Fig. 4).

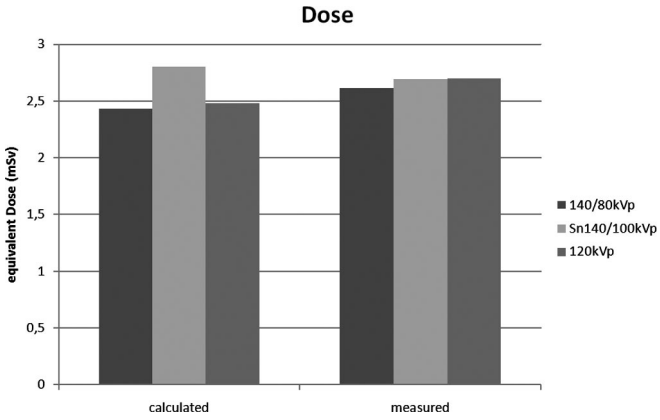

FIGURE 4. Comparison of radiation dose. Calculated doses result from the DLP of the patient protocol multiplied by a standard E/DLP conversion factor for the chest (0.017). Measured dose represent the exact dose, measured by TLDs and summarized taking the tissue weighting factor according to ICRP-103 into account.

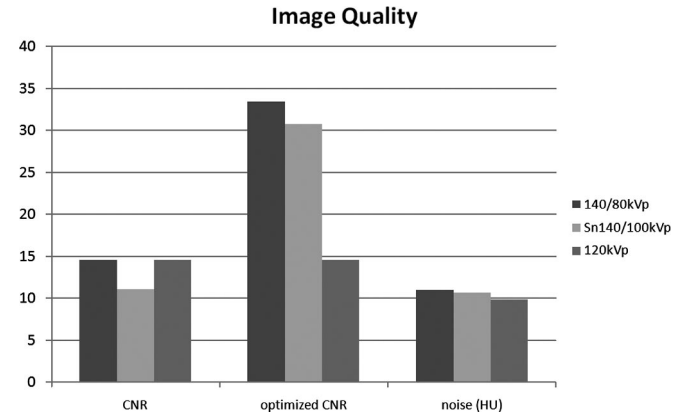

FIGURE 5. Comparison of different image quality measures. CNR values are defined as contrast enhancement divided by background noise. Optimized CNR is achieved with nonlinear blending algorithms, which use dual energy information to enhance the display of contrast material in the image.

Measured Dose

The doses measured in the individual organs with TLDs in the Alderson Rando phantom are listed in Table 2. After multiplication with the organ specific weighting factors according to IRCP 103,[24] the corresponding effective dose amounted to 2.61, 2.69, and 2.70 mSv, respectively, for the 140/80 kVp, the 140 Sn/100 kVp and the standard 120 kVp scan (Fig. 4).

Conversion Factors

As a basis to estimate patient doses as correctly as possible in a clinical setting, E/DLP conversion factors were calculated as ratio between the measured dose and the dose length product given in the patient protocol. The corresponding values were 0.0161 mSv/mGy*cm for the 140/80 kVp protocol, 0.0181 mSv/mGy*cm for the Sn140/100 kVp mode, and 0.0180 mSv/mGy*cm for the 120 kVp examination.

Image Noise

In the average images of the Sn140/100 kVp scan with 0.6 mm collimation reconstructed at 2 mm slice thickness, the image noise amounted to 10.7 HU. The 140/80 kVp scan with a collimation of 14 × 1.2 mm reconstructed with the same kernel and slice thickness resulted in a nearly equal image noise of 11.0 HU. With the standard 120 kVp chest protocol, the resulting noise was slightly lower with an average of 9.9 HU. Statistical analysis, using ANOVA did not reveal any statistically significant differences ($P = 0.342$) between the noise measured with the different protocols.

As noise is inversely related to the square root of dose,[27] an exactly equivalent noise as in the 120 kVp standard examination would require an estimated increase of 7% in dose at 140/80 kVp with 1.2 mm collimation or 11% at Sn140/100 kVp with 0.6 mm collimation.

Contrast to Noise Ratio

The general iodine contrast in the weighted average images was comparable to that in standard 120 kVp images. The corresponding CNR values amounted to 14.6 for the 140/80 kVp protocol, 11.1 for the Sn140/100 kVp protocol, and 14.6 for the 120 kVp scan, ie, there was no difference between the 140/80 kVp and 120 kVp spectra. The statistical analysis using ANOVA resulted in a significantly lower CNR for the Sn140/100 kVp ($P < 0.05$).

With the optimum contrast images which had been generated using the nonlinear blending algorithm, the contrast to noise ratio was considerably better with 30.7 for the Sn140/100 kVp protocol and 33.4 for the 140/80 kVp protocol, ie, 87 and 128% higher than with the standard 120 kVp spectrum ($P < 0.01$; cf. Fig. 5). There was no statistically significant difference between both Dual Energy protocols.

Regarding the spectral contrast, which is important for dual energy post processing, there were expected major differences between the 2 combinations of x-ray spectra. Mean difference in attenuation in the iodine syringe in the Sn140/100 kVp scan was 192 HU with a noise of 25.2 HU, resulting in a contrast to noise ratio of 7.62. The 140/80 kVp scan showed a difference in attenuation of 311 HU with a noise of 26.6 HU, resulting in a CNR of 11.7. The difference between both spectral combinations in CNR was statistically significant ($P < 0.01$).

DISCUSSION

In clinical routine DECT may offer additional, clinically relevant information. Several studies have meanwhile shown the benefits of this new imaging technique in clinical routine using an Food and Drug Administration approved software with several different applications.[7,8,11,15,16,19,28–31] On the other hand, recent publications[1] on lifetime attributable cancer risk of CT examinations have sparked off considerable awareness of radiation exposure,[32] its risks and appropriate indications.

Comparison of Dual Energy Protocols to Standard 120 kVp Chest Protocol

Our study tested 2 different Dual Energy chest protocols and compared them to a conventional 120 kVp protocol. With respect to radiation dose, the Dual Energy protocols resulted in 2.61 mSv and 2.69 mSv for the 140/80 kVp and Sn140/100 kVp, respectively, whereas the standard 120 kVp chest protocol amounted to 2.70 mSv. These objective dose measurements confirmed comparable doses for all 3 protocols. In this phantom study, image noise was not significantly different between these 3 protocols. Regarding CNR values, Sn140/100 kVp setting showed significantly lower values, if using the standard settings. However, these differences were outweighed using the nonlinear blending algorithm.

Comparison of 140/80 kVp and Sn140/100 kVp Setting

As the results for CNR and spectral contrast show, the hardened 140 kVp spectrum in combination with the tin filter and 100 kVp reference spectrum provides a smaller CNR and spectral contrast compared with 140/80 kVp setting. This difference is caused by the larger overlap of the spectra in the former setting and the higher mean energy which results in a loss of photoelectric effect. In contrast, the transmission of photons increases with this setting, which is a benefit for examinations in obese patients. Taking into account that the Alderson Rando phantom is relatively slim compared with the average patient in clinical routine, the advantages of the better transmission of the combination Sn140/100 kVp may not have been fully illustrated by the noise measurements in this study, but are quite evident in our clinical experience. In abdomen and chest, 1.2 mm collimation were used so far to compensate noise in 80 kVp acquisitions which is reflected by high noise using a 0.6 mm collimation in combination with a 140/80 kVp spectra.[8] The new tin filter and the hardened 140 kVp spectrum makes it possible to use 100 kVp as reference spectrum with the side effect of a weaker CNR as reflected in our measurements in iodine and water samples. In this respect, our measurement could not confirm the simulations by Primak et al,[23] from which one could expect an even improved CNR.

The different CT settings like collimation, tube current and reconstructed slice thickness must also be taken into account when comparing image noise between Sn140/100 kVp and 140/80 kVp setting.[33] The collimation applied at Sn140/100kVp protocol was 128 × 0.6 mm, which makes it possible to reconstruct thin slices of 0.6 mm thickness at the price of an increased background noise generated by the detector itself and the subsequent data processing. Practically this results in a difference of 0.8 HU more noise in comparison with a standard 120 kVp chest acquisition. A collimation of 14 × 1.2 mm used at 140/80 kVp scan decreases background noise by pooling the signals of 2 detector elements on one analog/digital converter and thus creates thicker layers.

Clinical Implications

Comparing Dual Energy protocols and standard pulmonary CTA protocols, the diagnostic relevance of an inferior image quality would not necessarily be outweighed by the spectral information, implying that average images should offer a similar quality and dose efficiency as standard CT acquisitions. The diagnostically relevant CNR values using optimized postprocessing imply that at least for angiographic examinations no additional dose is required and that linear blending algorithms can even improve CNR considerably at equivalent dose. This differs from the observations of Ho et al[34] who observed 2- to 3-fold doses for dual energy CT. However, their setup was based on a single source system using rapid voltage switching and contained neither a normalization of image noise nor of dose, so the lower energy spectrum was obtained additionally, whereas the higher energy spectrum was obtained with the same tube current time product as the single energy scan. In contrast, our approach was based on a dual source system with the same CT dose index for single and dual energy scans, so it is not surprising that the dose of the protocols is comparable.

A major problem of the first generation DSCT system is the restriction in FOV to 26 cm diameter which is caused by the geometrical arrangement of the second x-ray tube and the resulting smaller detector. For DECT, this represents a relevant limitation especially in the evaluation of lung perfusion and ventilation or the reconstruction of virtual noncontrast images of kidney and liver lesions.[11,16,22,28] With the design of the Siemens Definition Flash with a larger second detector at an increased angular offset, the 33 cm FOV resolves this limitation very well, because this diameter is sufficient to include the diagnostically relevant organs in most of patients.

The advantage of DECT is that it can offer additional information from a single scan on demand, like specific spectral information on contrast enhancement or an additional "virtual" noncontrast reconstruction.[22] Several studies have shown that, for example, the exact mapping of lung perfusion[29] or ventilation or a differentiation of kidney stones[8] is now feasible and offers clinical advantages without additional dose or limitations in image quality. This practical value only applies if DECT routinely replaces standard protocols, and knowing that the Dual Energy protocols are clinically feasible with comparable radiation dose, they can be used as standard setting for a wide range of applications.

Limitations of the Study

Ideally, noise measurements and CNR comparisons should be performed exactly in the center of the gantry, which is not possible in the Alderson phantom with its antropomorphic anatomy. As we acquired our measurements at equivalent positions with all 3 protocols, the comparison should remain valid. Also, image noise is not homogeneous over the whole FOV but generally decreases in the periphery, which may increase contrast to noise ratio. We did not specifically address this issue with our measurements. Still, as we performed our measurements with the Alderson phantom centered exactly in the gantry for the different scan protocols and identically positioned regions of interest, the comparison should be valid. We also only evaluated syringes with water and iodine in high concentration to determine CNR. From these experiments, conclusions can only be drawn for angiographic examinations in which similar iodine concentrations are achieved in the vessel, but not for other clinical issues such as the detection of focal lesions in solid organs. Another limitation is that we applied different collimations with the different spectral combinations. The simple reason is that the 80 kVp spectrum yields insufficient transmission in average size adult patients with 0.6 mm collimation, while 100 kVp image noise is acceptable with the Sn140/100 kVp combination, and then it is clinically useful to apply the thinner collimation. Thus, our measurements reflect clinically applicable scan parameters with the different spectral combinations.

CONCLUSION

DECT of the chest is feasible without additional dose. There is no significant difference in image noise, while CNR can be doubled with optimized dual energy CT reconstructions. Regarding the total applied dose, the possibility of virtual noncontrast reconstructions can even reduce the dose by a factor of 2 if an unenhanced scan is omitted. With a restricted collimation of 14 × 1.2 mm, 140/80 kVp examinations lead to approximately the same image noise and radiation dose but a higher Dual Energy contrast and CNR compared with 140Sn/100 kVp acquisitions with a finer collimation of 128 × 0.6 mm. Overall, image quality, image noise and dose are comparable to a standard 120 kVp chest protocol, and virtual unenhanced reconstructions and a wide range of specific applications like eg, ventilation or perfusion imaging can be chosen on demand.

REFERENCES

1. Einstein AJ, Henzlova MJ, Rajagopalan S. Estimating risk of cancer associated with radiation exposure from 64-slice computed tomography coronary angiography. *JAMA*. 2007;298:317–323.
2. Lechel U, Becker C, Langenfeld-Jager G, et al. Dose reduction by automatic exposure control in multidetector computed tomography: comparison between measurement and calculation. *Eur Radiol*. 2009;19:1027–1034.

3. Flohr TG, McCollough CH, Bruder H, et al. First performance evaluation of a dual-source CT (DSCT) system. *Eur Radiol*. 2006;16:256–268.
4. Petersilka M, Bruder H, Krauss B, et al. Technical principles of dual source CT. *Eur J Radiol*. 2008;68:362–368.
5. Johnson TR, Nikolaou K, Wintersperger BJ, et al. Dual-source CT cardiac imaging: initial experience. *Eur Radiol*. 2006;16:1409–1415.
6. Johnson TR, Nikolaou K, Busch S, et al. Diagnostic accuracy of dual-source computed tomography in the diagnosis of coronary artery disease. *Invest Radiol*. 2007;42:684–691.
7. Johnson TR, Krauss B, Sedlmair M, et al. Material differentiation by dual energy CT: initial experience. *Eur Radiol*. 2007;17:1510–1517.
8. Graser A, Johnson TR, Bader M, et al. Dual energy CT characterization of urinary calculi: initial in vitro and clinical experience. *Invest Radiol*. 2008; 43:112–119.
9. Scheffel H, Stolzmann P, Frauenfelder T, et al. Dual-energy contrast-enhanced computed tomography for the detection of urinary stone disease. *Invest Radiol*. 2007;42:823–829.
10. Thomas C, Krauss B, Tsiflikas I, et al. Differentiation of urinary calculi with dual energy CT: effect of spectral shaping by high energy tin filtration. *Invest Radiol.* In press.
11. Graser A, Johnson TR, Chandarana H, et al. Dual energy CT: preliminary observations and potential clinical applications in the abdomen. *Eur Radiol*. 2009;19:13–23.
12. Robinson E, Babb J, Chandarana H, et al. Dual source dual energy MDCT: preliminary observations comparing 80 kVp and weighted average 120 kVp data for conspicuity of hypo-vascular liver metastases. *Invest Radiol.* In press.
13. Graser A, Staehler M, Macari M, et al. Single-phase dual energy CT allows for characterization of renal masses as benign or malignant. *Invest Radiol.* In press.
14. Zhang L, Peng J, Wu SY, et al. Dual source dual energy CT of acute myocardial infarction: correlation with histopathological findings in a canine model. *Invest Radiol.* 2010;45:290–297.
15. Chae EJ, Seo JB, Goo HW, et al. Xenon ventilation CT with a dual-energy technique of dual-source CT: initial experience. *Radiology*. 2008;248:615–624.
16. Thieme SF, Becker CR, Hacker M, et al. Dual energy CT for the assessment of lung perfusion—correlation to scintigraphy. *Eur J Radiol*. 2008;68:369–374.
17. Krissak R, Henzler T, Reichert M, et al. Enhanced visualization of lung vessels for diagnosis of pulmonary embolism using dual energy CT angiography. *Invest Radiol.* 2010;45:341–346.
18. Chae E, Seo J, Lee J, et al. Xenon ventilation imaging using dual energy CT in asthmatics: initial experience. *Invest Radiol.* 2010;45:354–361.
19. Morhard D, Fink C, Graser A, et al. Cervical and cranial computed tomographic angiography with automated bone removal: dual energy computed tomography versus standard computed tomography. *Invest Radiol*. 2009;44: 293–297.
20. Sommer WH, Johnson TR, Becker CR, et al. The value of dual-energy bone removal in maximum intensity projections of lower extremity computed tomography angiography. *Invest Radiol*. 2009;44:285–292.
21. Lell MM, Kramer M, Klotz E, et al. Carotid computed tomography angiography with automated bone suppression: a comparative study between dual energy and bone subtraction techniques. *Invest Radiol*. 2009;44:322–328.
22. Graser A, Johnson TR, Hecht EM, et al. Dual-energy CT in patients suspected of having renal masses: can virtual nonenhanced images replace true nonenhanced images? *Radiology*. 2009;252:433–440.
23. Primak AN, Ramirez Giraldo JC, Liu X, et al. Improved dual-energy material discrimination for dual-source CT by means of additional spectral filtration. *Med Phys*. 2009;36:1359–1369.
24. The 2007 Recommendations of the International Commission on Radiological Protection. ICRP publication 103. *Ann ICRP.* 2007;37:1–332.
25. Holmes DR III, Fletcher JG, Apel A, et al. Evaluation of non-linear blending in dual-energy computed tomography. *Eur J Radiol*. 2008;68:409–413.
26. Huda W, Ogden KM, Khorasani MR. Converting dose-length product to effective dose at CT. *Radiology*. 2008;248:995–1003.
27. Irie T, Inoue H. Individual modulation of the tube current-seconds to achieve similar levels of image noise in contrast-enhanced abdominal CT. *Am J Roentgenol*. 2005;184:1514–1518.
28. Thieme SF, Johnson TR, Lee C, et al. Dual-energy CT for the assessment of contrast material distribution in the pulmonary parenchyma. *Am J Roentgenol*. 2009;193:144–149.
29. Pontana F, Faivre JB, Remy-Jardin M, et al. Lung perfusion with dual-energy multidetector-row CT (MDCT): feasibility for the evaluation of acute pulmonary embolism in 117 consecutive patients. *Acad Radiol*. 2008;15:1494–1504.
30. Zhang Y, Zhang ZH, Jin ZY, et al. [Radiological features of dual-energy CT lung perfusion imaging in patients with acute pulmonary embolism: comparison with CT pulmonary angiography]. *Zhongguo Yi Xue Ke Xue Yuan Xue Bao*. 2009;31:166–170.
31. Stolzmann P, Kozomara M, Chuck N, et al. In vivo identification of uric acid stones with dual-energy CT: diagnostic performance evaluation in patients. *Abdom Imaging.* In press.
32. Brenner DJ, Hall EJ. Computed tomography—an increasing source of radiation exposure. *N Engl J Med*. 2007;357:2277–2284.
33. Brink JA. Technical aspects of helical (spiral) CT. *Radiol Clin North Am*. 1995;33:825–841.
34. Ho LM, Yoshizumi TT, Hurwitz LM, et al. Dual energy versus single energy MDCT: measurement of radiation dose using adult abdominal imaging protocols. *Acad Radiol*. 2009;16:1400–1407.